Inverse design of broadband epsilon-near-zero metasurface with nanoscale airtube superlattice based on the Bergman-Milton spectral representation

Lei Sun [1], Kin Wah Yu,[2] and Guo Ping Wang[1,*]

[1]*Lab of Artificially Micro- and Nano-structured Materials and Devices for Photonics, Institute of Microscale Optoelectronics (IMO), Shenzhen University, 3688 Nanhai Ave., Shenzhen 518060, People's Republic of China*
[2]*Department of Physics, The Chinese University of Hong Kong, Shatin, N.T., Hong Kong*

A metal-dielectric composite metasurface of the broadband epsilon-near-zero property is designed with the nanoscale airtube superlattice microstructure embedded in the metallic host. The design strategy rigorously starts from the theoretical analysis on the spectral representation of effective permittivity in quasistatic conditions for the Hashin-Shtrikman coated-cylinder microstructure, then improves in full-wave conditions for the nanoscale airtube superlattice microstructure. Through the computational simulations, the correctness and robustness of the strategy are verified and the broadband epsilon-near-zero property of the designed metasurface is demonstrated. Furthermore, the physical mechanism behind the broadband epsilon-near-zero property, including the potential application in broadband deep subwavelength electromagnetic wave tunneling, is also straightforwardly revealed.

I. INTRODUCTION

Metamaterials are a kind of artificial composites, rationally constructed by tailored building blocks periodically or nonperiodically, leading to extraordinary macroscopic effective medium properties that do not exist in nature [1–4]. In all kinds of metamaterials, the electromagnetic metamaterials, which are structured with subwavelength metal/dielectric components and show unusual effective electric permittivity and magnetic permeability with respect to the probing electromagnetic wave, imply great potentials in electromagnetic field control [5]. Therefore, they quickly emerge into the focus of the exploration in fundamental scientific researches and engineering applications [6–14]. As a significant example, the epsilon-near-zero (ENZ) metamaterials with the near-zero permittivity are of vastly important applications at microwave and optical frequencies, such as light tunneling through distorted channels, highly directive emission, light trapping, nonlinear optical processes, enhanced nonreciprocal and nonlocal responses, and quantum information procedures, since the near-zero permittivity can decouple not only the electricity and magnetism, but also the spatial (wavelength) and temporal (frequency) field variations of the electromagnetic wave [15–24]. Consequently, various strategies are proposed to construct the ENZ metamaterials at different desired operating frequencies. Especially, in order to overcome the disadvantage of a single operating frequency and enrich the practical application, great attempts are proposed to construct the broadband ENZ metamaterials, such as topology optimization, and inverse design. In general, the topology optimization is a forward method that optimizes a set of parameters of a microstructure in certain constraints to obtain the desired macroscopic effective medium properties [25–29],

while the inverse design is an approach that defines the desired macroscopic effective medium properties and retrieves a microstructure exhibiting them [30–35]. As a kind of computer-aided design, the topology optimization is similar to the method of exhaustion, which is cumbersome and cannot directly reveal the physical mechanism behind. In contrast, the inverse design is efficient but can be quite difficult in dealing with inverse problems for complex microstructures. Therefore, previous studies about the inverse design mainly focus on numerical solutions or analytical solutions with respect to specific ideal microstructures, e.g., the Hashin-Shtrikman coated-sphere microstructure [36]. For practical microstructure, explorations about the inverse design are still insufficient.

Regarding the problems, the inverse design of a broadband ENZ metasurface (i.e., a kind of planar metamaterials) with nanoscale airtube superlattice microstructure is studied and demonstrated in this work, through explorations of the inverse problem by both rigorous theoretical analysis in quasistatic conditions and numerical analysis in full-wave conditions. In general, the inverse design is analytically explored at first through the Bergman-Milton spectral representation [37–44] of effective permittivity for the ideal two-dimensional Hashin-Shtrikman coated-cylinder microstructure in quasistatic conditions, and the precise results of the inverse problem are verified via the finite element numerical simulations in full-wave conditions. Subsequently, according to the rigorous results of the inverse problem and the optical nonlocality analysis results in full-wave conditions, the Hashin-Shtrikman microstructure is replaced by the nanoscale airtube superlattice microstructure to construct the broadband ENZ metasurface. Finally, the broadband ENZ property of the designed metasurface is confirmed, while the physical mechanism of the broadband ENZ response, including the potential application in broadband deep subwavelength electromagnetic wave tunneling, is revealed via the mode analysis method.

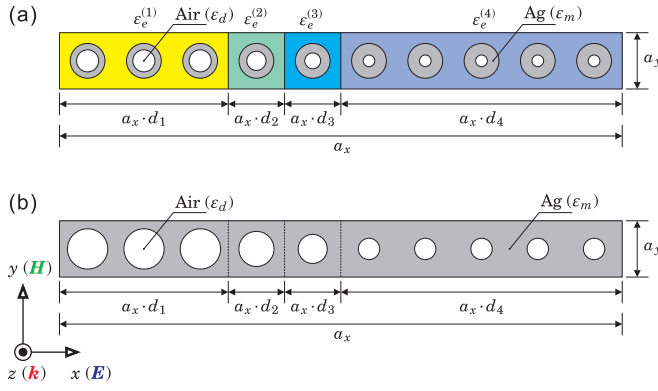*Corresponding author: gpwang@szu.edu.cn

FIG. 1. Cross section of the four-meta-atom unit cell with (a) the Hashin-Shtrikman coated cylinder microstructure and (b) the nanoscale airtube superlattice microstructure in the broadband ENZ metasurface.

II. MICROSTRUCTURE OF THE BROADBAND ENZ METASURFACE

In general, the broadband ENZ metasurface is periodically constructed with identical unit cells in both x and y direction. All unit cells are of the cross section $a_x \times a_y$ in the x-y plane and the thickness h_z in the z direction just as schematically depicted in Fig. 1. The scales of the unit cell are less than the wavelength of the x-polarized probing electromagnetic wave propagating along the z direction. Every unit cell is a metal-dielectric (of the permittivity ε_m and ε_d, respectively) composite, which is sophisticatedly designed in order to possess the broadband ENZ property in the desired operating frequency range. Therefore, the whole metasurface will be broadband ENZ response in the same operating frequency range. In this work, the noble metal Ag (silver) that is of the permittivity from experimental results [45] is selected as the metal component, while the air of the unit permittivity is selected as the dielectric component.

In detail, every unit cell contains N meta-atoms (e.g., $N = 4$ in this work) of the length fraction d_i, respectively. The filling ratios of the metal and the dielectric components in the ith meta-atom are individually denoted as $f_m^{(i)}$ and $f_d^{(i)}$, which satisfy the summation rule of $f_m^{(i)} + f_d^{(i)} \equiv 1$. With respect to the probing electromagnetic wave, different meta-atoms will possess the ENZ response at different frequencies in the operating frequency range. By properly arranging the length fractions and the component filling ratios, the meta-atoms can efficiently couple together; thus the unit cell will possess the broadband ENZ property. In this work, the inverse design of the broadband ENZ metasurface is rigorously studied in theory for the unit cell in a quasistatic condition, in which all meta-atoms are of the Hashin-Shtrikman coated-cylinder microstructure [Fig. 1(a)]. Subsequently, according to the solutions of the inverse problem, the unit cell with meta-atoms of the nanoscale airtube lattice microstructure, i.e., the nanoscale airtube superlattice microstructure [Fig. 1(b)], is designed and numerically demonstrated in the full-wave condition.

III. THEORETICAL ANALYSIS OF THE INVERSE DESIGN

In order to obtain the exact solutions of the inverse problem, the theoretical analysis of the inverse design starts with

the Hashin-Shtrikman microstructure, since the effective permittivity of the meta-atom $\varepsilon_e^{(i)}$ of the Hashin-Shtrikman microstructure can be exactly obtained via the Maxwell-Garnett equation [46]

$$\frac{\varepsilon_e^{(i)} - \varepsilon_m}{\varepsilon_e^{(i)} + \varepsilon_m} = \left(1 - f_m^{(i)}\right)\frac{\varepsilon_d - \varepsilon_m}{\varepsilon_d + \varepsilon_m} \tag{1}$$

as a function of the filling ratio of the metal component. Furthermore, the effective permittivity (in the x direction) of the unit cell ε_e can be determined as

$$\varepsilon_e = \left[\sum_{i=1}^{N} \frac{d_i}{\varepsilon_e^{(i)}}\right]^{-1} \tag{2}$$

associated with both the filling ratios of the metal component and the length fractions of the meta-atoms. Obviously, it is difficult to achieve the broadband ENZ unit cell by directly tuning the filling ratios of the metal component and the length fractions. However, by introducing the material parameter $s \equiv \varepsilon_d/(\varepsilon_d - \varepsilon_m)$, the effective permittivity of each meta-atom in Eq. (1) can be mapped into the spectral space and rewritten as

$$\frac{\varepsilon_e^{(i)}}{\varepsilon_d} = \frac{s-1}{s}\frac{s - f_m^{(i)}/2}{s - \left(2 - f_m^{(i)}\right)/2} \tag{3}$$

in the Bergman-Milton spectral representation format. Therefore, the effective permittivity of the unit cell in Eq. (2) can be represented as

$$\frac{\varepsilon_d}{\varepsilon_e} = \frac{s}{s-1}\left[1 - \sum_{i=1}^{N}\frac{(1 - f_m^{(i)})d_i}{s - f_m^{(i)}/2}\right] \tag{4}$$

based on Eq. (3) and the summation rule of the length fraction $\sum_{i=1}^{N} d_i \equiv 1$. On the other hand, the effective permittivity of the unit cell can also be directly expressed as

$$\frac{\varepsilon_d}{\varepsilon_e} = \frac{s}{s-1}\prod_{i=1}^{N}\frac{s - s_i}{s - z_i}$$

$$= \frac{s}{s-1}\left[1 - \sum_{i=1}^{N}\frac{\prod_{j=1}^{N}(s_j - z_i)}{(s - z_i)\prod_{j \neq i}^{N}(z_j - z_i)}\right] \tag{5}$$

in the Bergman-Milton spectral representation format, where the pole(s_i)-zero(z_i) series obeys the following restriction:

$$0 < z_1 < s_1 < \cdots < z_i < s_i < \cdots < z_N < s_N < 1. \tag{6}$$

According to Eq. (5), it is clear that the effective permittivity of the unit cell will approach zero when the material parameter gets close to each zero. Therefore, the broadband ENZ unit cell can be simply constructed in the spectral space by properly arranging the pole-zero series. Noting that, to the same unit cell, Eqs. (4) and (5) must provide the same results, thus there is the inverse problem

$$\sum_{i=1}^{N}\frac{(1 - f_m^{(i)})d_i}{s - f_m^{(i)}/2} = \sum_{i=1}^{N}\frac{\prod_{j=1}^{N}(s_j - z_i)}{(s - z_i)\prod_{j \neq i}^{N}(z_j - z_i)} \tag{7}$$

connecting the pole-zero series and the filling ratios of the metal component and the length fractions, with the simple

solutions as

$$f_m^{(i)} = 2z_i, \tag{8}$$

$$d_i = \frac{\prod_{j=1}^{N}(s_j - z_i)}{(1 - 2z_i)\prod_{j \neq i}^{N}(z_j - z_i)}. \tag{9}$$

However, regarding the constraints on the filling ratios of the metal component $0 < f_m^{(i)} < 1$ and the length fractions $0 < d_i < 1$ and the summation rule of the length fractions $\sum_{i=1}^{N} d_i \equiv 1$, there are additional restrictions on the pole-zero series

$$0 < z_i < 1/2, \tag{10}$$

$$\prod_{i=1}^{N} \frac{1 - 2s_i}{1 - 2z_i} \equiv -1 \tag{11}$$

besides the essential restriction in Eq. (6).

In principle, any pole-zero series that satisfies the restrictions of Eqs. (6), (10), and (11) will lead to a possible configuration of the broadband ENZ unit cell based on Eqs. (8) and (9). However, an efficient strategy is still worth being studied. For instance, regarding a desired operating frequency range $[\omega_{\text{initial}}, \omega_{\text{final}}]$, the zero series can be simply arranged as an arithmetic sequence

$$z_i = z_1 + (i - 1)\Delta \quad (0 < z_i < 1/2 \quad \text{and} \quad i = 1, 2, \dots, N) \tag{12}$$

for the sake of mathematical convenience, where the common difference reads $\Delta = (z_N - z_1)/(N - 1)$ with the first zero $z_1 = \text{Re}[\varepsilon_d/(\varepsilon_d - \varepsilon_m)]_{\omega = \omega_{\text{initial}}}$ and the last zero $z_N = \text{Re}[\varepsilon_d/(\varepsilon_d - \varepsilon_m)]_{\omega = \omega_{\text{final}}}$. Correspondingly, with respect to the restrictions on the pole-zero series, the related pole series can be arranged as

$$s_i = \begin{cases} \dfrac{(\sqrt[N-1]{\rho} - 1) + 2z_i}{2\sqrt[N-1]{\rho}} & (i = 1, 2, 3, \dots, N), \\[3mm] \dfrac{1}{2} + \dfrac{\rho(1 - 2z_N)}{2} & (i = N), \end{cases} \tag{13}$$

in which the variable ρ is confined in the range of

$$1 < \rho < \rho_{\text{max}} = \frac{1}{2}\left[1 + \frac{2\Delta}{(1 - 2z_1) - 2\Delta}\right]^{N-1}. \tag{14}$$

According to experience, one suggested value of the variable ρ is $\rho = (1 + \rho_{\text{max}})/2$, which is applied throughout this work. Consequently, the filling ratios of the metal component and the length fractions can be determined according to the solutions of the inverse problem. As an exact example, regarding the operating frequency from 822.194 THz to 891.268 THz, the configuration of the Ag-air composed four-meta-atom broadband ENZ unit cell can be constructed as based on the strategy above. According to the Maxwell-Garnett equation in Eq. (1), each meta-atom of the corresponding filling ratios in Table I will possesses the ENZ property at a single frequency in the operating frequency range, while the length fractions will lead to the coupling among all meta-atoms via Eq. (2) and form the broadband ENZ unit cell. It is worth mentioning that, in order to simplify

TABLE I. Configuration of the Ag-air four-meta-atom broadband ENZ unit cell.

Meta-atoms	Filling ratio of Ag $f_m^{(i)}$	Filling ratio of air $f_d^{(i)}$	Length fraction d_i	Approximate length fraction d_i
$i = 1$	0.597	0.403	0.265	0.3
$i = 2$	0.694	0.306	0.094	0.1
$i = 3$	0.791	0.209	0.110	0.1
$i = 4$	0.887	0.113	0.531	0.5

the further construction of the broadband ENZ unit cell with the nanoscale airtube lattice microstructure, the length fractions obtained from the strategy are slightly approximated and applied in the following sections, which will not dramatically affect the broadband ENZ response.

IV. BROADBAND ENZ UNIT CELLS WITH HASHIN-SHTRIKMAN MICROSTRUCTURE

Regarding the exact microstructure of each meta-atom in the broadband ENZ unit cell, the straightforward profile is the Hashin-Shtrikman microstructure, since the microstructure precisely agrees with the Maxwell-Garnett equation in Eq. (1). Figure 2(a) demonstrates the effective permittivity of the designed broadband ENZ unit cell with the Hashin-Shtrikman microstructure according to the configuration in Table I. In general, the broadband ENZ unit cell is of a deep-subwavelength cross section $a_x \times a_y = 1$ nm $\times$ 10 nm and the thickness $h_z = 65$ nm that is greater than the skin depth of Ag with respect to the probing electromagnetic wave in the operating frequency range. The coated cylinders are of the outer radius that is about $r_{\text{out}} = 0.3a_y$ in all meta-atoms and of the inner radius that is proportional to the filling ratios of the components in the meta-atom. The theoretical effective permittivity of the broadband ENZ unit cell is calculated from Eq. (2) and indicated by solid curves. Besides that, in the full wave condition, the effective permittivity can be retrieved from the transmission and reflection coefficients [47], which are calculated by the finite element method with respect to the probing electromagnetic wave, and the results are indicated by dashed curves. It is obvious that all results show that the unit cell possesses a near-zero effective permittivity in the operating frequency range, and the retrieved results almost coincident with the theoretical prediction. However, due to the diffraction of the probing electromagnetic wave on the surface of the unit cell, the accuracy of the retrieve algorithm will be reduced. Therefore, small fluctuations between the theoretical and the retrieved effective permittivity can be observed. In order to avoid the unwanted diffraction, the eigenmode analysis method is applied to determine the effective permittivity in the full wave condition, and the results are denoted by circles. Clearly, the effective permittivity based on the eigenmode analysis is exactly coincident with the theoretical results. Furthermore, the eigenmode analysis method can even reveal the physical mechanism behind the broadband ENZ property. Figure 2(b) displays the eigenmodes at five frequencies, where the effective permittivity is close to zero as marked by arrows
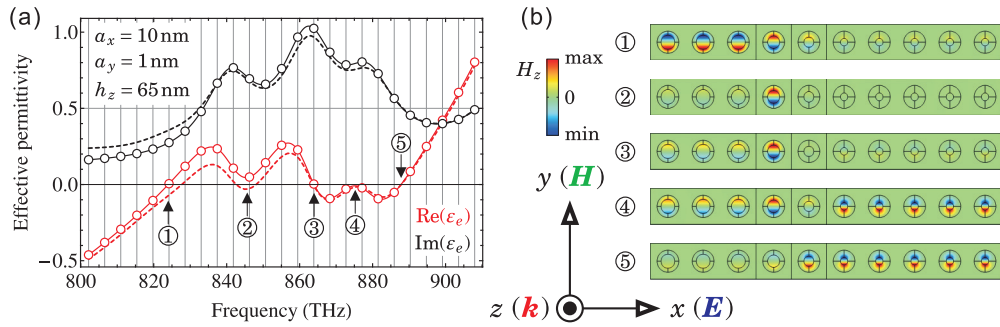
FIG. 2. (a) Effective permittivity of the broadband ENZ unit cell with the Hashin-Shtrikman coated cylinder microstructure based on theoretical calculations (solid curves), the transmission and reflection coefficients retrieve algorithm (dashed curves), and the mode analysis (circles), respectively. (b) Profiles of the eigenmode at the frequency, where the effective permittivity is close to zero, displayed by the z component of the magnetic field.

in Fig. 1(a). The profiles of the eigenmodes are demonstrated by the z component of the magnetic field. It is clear that, at the increasing of the frequency, the meta-atoms are successively activated due to the well-designed coupling effect among all meta-atoms. Therefore, the whole unit cell exhibits the broadband ENZ property to the probing electromagnetic wave.

V. BROADBAND ENZ UNIT CELLS WITH NANOSCALE AIRTUBE SUPERLATTICE

Although the Hashin-Shtrikman microstructure precisely conforms to the Maxwell-Garnett equation, it is far from practical. To overcome this disadvantage, the nanoscale airtube lattice is suggested to replace the Hashin-Shtrikman microstructure, since in general the effective permittivity of the airtube lattice approximately meets the prediction of the Maxwell-Garnett equation. Moreover, another advantage is that the electromagnetic wave propagating in such a structure does not suffer radiative losses [48]. However, due to the significant variation of the electromagnetic wave on the scale of the period of the lattice, i.e., the optical nonlocality, the effective permittivity of the airtube lattice may notably deviate from the theoretical prediction in certain conditions. Therefore, it is worth exploring the applicability of the Maxwell-Garnett equation on the airtube lattice. Considering the polarization independence of the Maxwell-Garnett equation, the nanoscale airtube lattice for each meta-atom should be of the same deep subwavelength period in both x and y directions as depicted in Fig. 3(a). The thickness of the airtube lattice is still set as $h_z = 65$ nm which is greater than the skin depth of Ag with respect to the probing electromagnetic wave in the investigating frequency range. In the full-wave condition, the effective permittivity of the airtube lattice is retrieved from the transmission and reflection coefficients and compared with the theoretical results from the Maxwell-Garnett equation. Figures 3(b)–3(h) display the comparison by denoting the theoretical results as solid curves and the retrieved results as dashed curves. With the increase of the filling ratios of the air component from $f_{air} = 0.1$ to 0.7, it is easy to find that the Maxwell-Garnett equation works well with small filling ratios, i.e., about $f_{air} \leqslant 0.4$, and steeply loses accuracy after that. This is because the Maxwell-Garnett equation is derived by treating the inclusions as dipole moments. Once

the inclusions cannot be treated as dipole moments, the Maxwell-Garnett equation will be invalid. According to the configuration in Table I, the designed broadband ENZ unit cell satisfies the requirement.

As a consequence, each meta-atom can be constructed by the nanoscale airtube lattice in the host media of Ag based on the configuration in Table I; thus the broadband ENZ unit cell forms the airtube superlattice microstructure. Figure 4 displays the results of the broadband ENZ unit cell with the airtube superlattice microstructure of different scales. Take the results of Figs. 4(a) and 4(b) as an example. With respect to the designed airtube superlattice unit cell of the cross section $a_x \times a_y = 1$ nm $\times$ 10 nm and the thickness $h_z = 65$ nm, the effective permittivity retrieved from the transmission and reflection coefficients is denoted as dashed curves. Compared with the theoretical results that are denoted as solid curves, it is clear that the retrieve effective permittivity is close to zero in the operating frequency range and of small deviations from the theoretical results. In contrast with the Hashin-Shtrikman microstructure, the deviations of the airtube superlattice unit cell not only result from the diffraction of the probing electromagnetic wave on the surface of the unit cell but also arise from the reduced coupling efficiency among the meta-atoms because of the indefinite interfaces between adjacent meta-atoms. Similar results can also be found in the effective permittivity based on the eigenmode analysis denoted as dashed curves with circles. In addition, the profiles of the eigenmodes at the frequencies where the effective permittivity is close to zero are explored and displayed in Fig. 4(b) by the z component of the magnetic field. It is obvious that each airtube acts as a dipole moment excited by the probing electromagnetic wave; thus the Maxwell-Garnett equation can well predict the effective permittivity. Also, the well-designed coupling effect makes sure that the meta-atoms are stimulated in succession in order to achieve the broadband ENZ response with the whole broadband ENZ unit cell. Furthermore, the broadband ENZ response still can be achieved in the unit cell of different scales just as the results depicted in Fig. 4(c) for a broadband ENZ unit cell with all edges of the cross section doubled, in which the same physical mechanism still dominates the broadband ENZ response as shown in Fig. 4(d). It is worth stressing that the enlarged cross section of the unit cell also enhances the diffraction
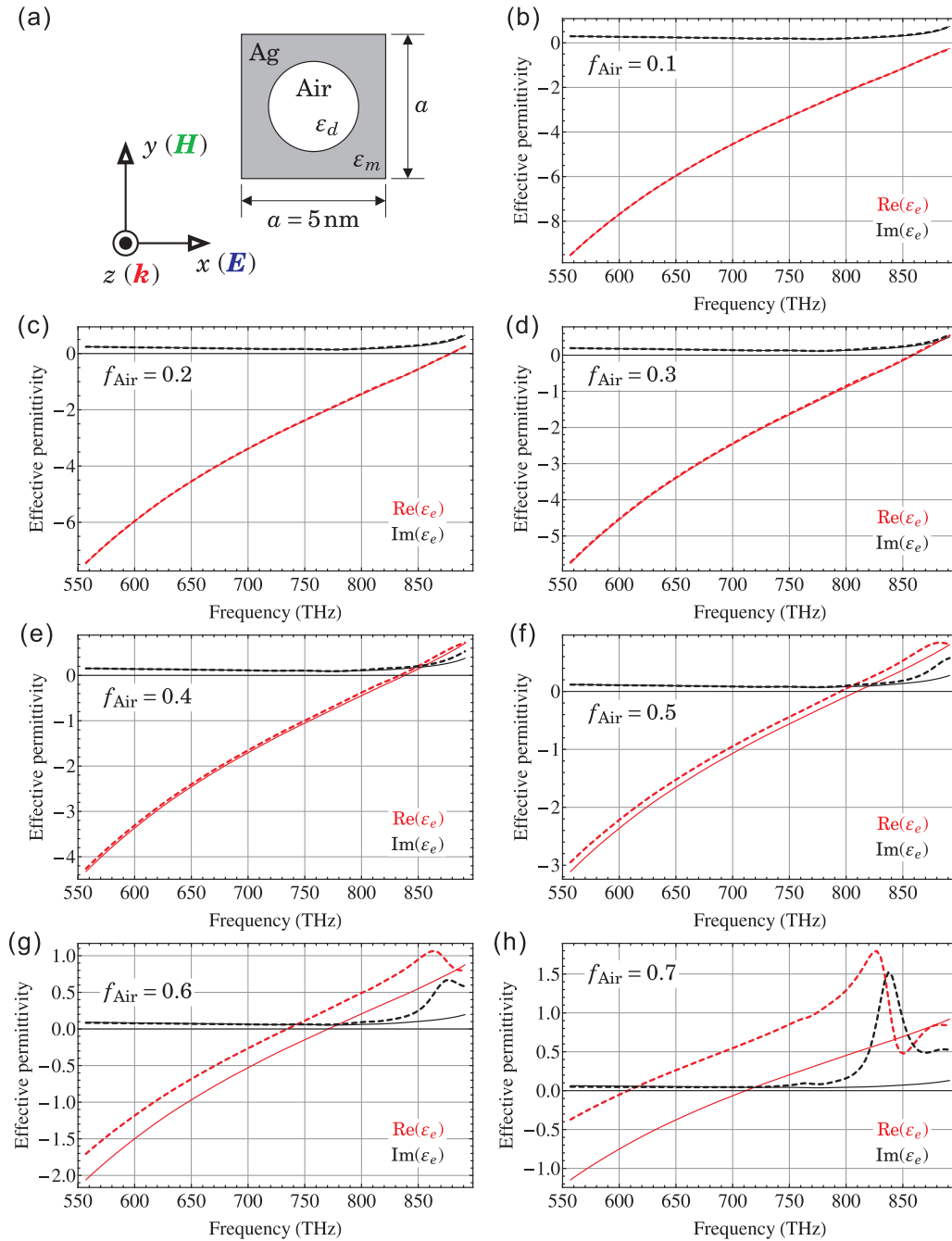
FIG. 3. (a) Cross section of the period unit of the nanoscale airtube lattice. (b)–(h) Effective permittivity of the nanoscale airtube lattice based on theoretical calculations (solid curves) and the transmission and reflection coefficients retrieve algorithm (dashed curves), with the filling ratios of the air component from $f_{air} = 0.1$ to 0.7, respectively.

of the probing electromagnetic wave from the surface of the unit cell that leads to the increased deviations in the retrieved effective permittivity as demonstrated by dashed curves in Fig. 4(c). However, regarding the effective permittivity based on the eigenmode analysis, the results are almost unchanged. Furthermore, it notes that the operating frequency range is extended compared with the theoretical results according to the effective permittivity based on the eigenmode analysis as shown in Figs. 4(a) and 4(c). This is coincident with the results in Fig. 3(e) that the filling ratio of the air component in the first meta-atom of the unit cell is slightly greater than 0.4 and

will shift the ENZ frequency to a lower frequency. Therefore, the design strategy possesses well-behaved robustness. It is worth emphasizing that the unit cells discussed above are all in the deep subwavelength scale in the operating frequency range. However, the mode analysis clearly demonstrates that the electromagnetic wave can still propagate through the airtube superlattice, which clarifies that the broadband ENZ unit cell possesses a great potential application in broadband deep subwavelength electromagnetic wave tunneling, i.e., broadband information transmission beyond the diffraction limit.
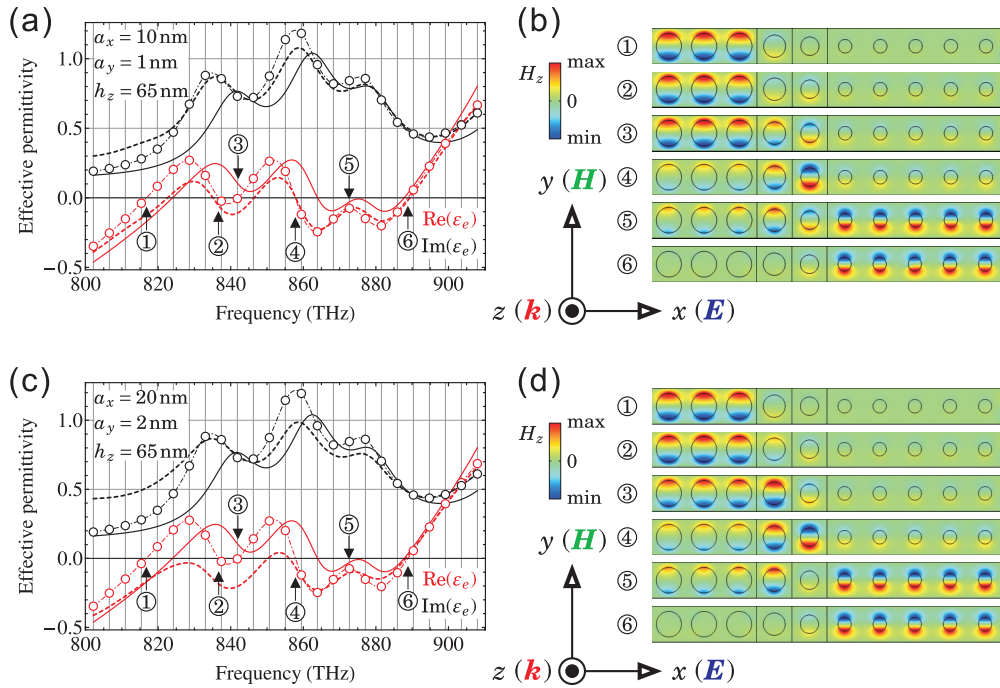
FIG. 4. For the broadband ENZ unit cell with the nanoscale airtube superlattice microstructure of the cross sections $a_x \times a_y = 10$ nm $\times$ 1 nm and 20 nm $\times$ 2 nm, (a), (c) the effective permittivity of the unit cell based on theoretical calculations (solid curves), the transmission and reflection coefficients retrieve algorithm (dashed curves), and the mode analysis (circles); (b), (d) the profiles of the eigenmode at the frequency, where the effective permittivity is close to zero, displayed by the z component of the magnetic field.

VI. CONCLUSIONS

To conclude, a metal-dielectric composed broadband ENZ metasurface is designed according to a sophisticated inverse design strategy based on the Bergman-Milton spectral representation of effective permittivity. On the basis of the strategy, the ideal unit cell for the broadband ENZ metasurface is first constructed with the Hashin-Shtrikman coated-cylinder microstructure and demonstrated via rigorous theoretical analysis in quasistatic conditions and computational simulations in full-wave conditions. Subsequently, a practical unit cell for the broadband ENZ metasurface is proposed by introducing the nanoscale airtube superlattice microstructure embedded in the metallic host medium under the guidance of the optical nonlocality analysis, in order to overcome the disadvantage of the Hashin-Shtrikman coated-cylinder microstructure in realistic applications. Compared with the theoretical results, the effective permittivity of the practical unit cell calculated via the computational simulations in full wave conditions

does meet the theoretical prediction. By means of the mode analysis, the physical mechanism behind the broadband ENZ metasurface is clearly revealed as the deep subwavelength electromagnetic wave tunneling through the nanoscale airtube superlattice at the frequency where the effective permittivity is close to zero. The unique property directly implies a great application potential of the broadband ENZ metasurface in the field of the broadband information transmission beyond the diffraction limit. Finally, the broadband ENZ property of the metasurface may raise great applications in nonlinear optical processes, enhanced nonreciprocal and nonlocal responses, quantum information procedures, and other fields.

[1] S. Jahani and Z. Jacob, Nat. Nanotechnol. **11**, 23 (2016).

[2] S. A. Cummer, J. Christensen, and A. Alù, Nat. Rev. Mater. **1**, 16001 (2016).

[3] N. Lazarides and G. P. Tsironis, Phys. Rep. **752**, 1 (2018).

[4] M. Kadic, G. W. Milton, M. van Hecke, and M. Wegener, Nat. Rev. Phys. **1**, 198 (2019).

[5] K. Fan and W. J. Padilla, Mater. Today **18**, 39 (2015).

[6] A. Silva, F. Monticone, G. Castaldi, V. Galdi, A. Alù, and N. Engheta, Science **343**, 160 (2014).

[7] C. D. Giovampaola and N. Engheta, Nat. Mater. **13**, 1115 (2014).

[8] W. Gao, M. Lawrence, B. Yang, F. Liu, F. Fang, B. Béri, J. Li, and S. Zhang, Phys. Rev. Lett. **114**, 037402 (2015).

[9] A. D. Neira, N. Olivier, M. E. Nasir, W. Dickson, G. A. Wurtz, and A. V. Zayats, Nat. Commun. **6**, 7757 (2015).

[10] M. Xiao, Q. Lin, and S. Fan, Phys. Rev. Lett. **117**, 057401 (2016).

[11] Y. Xu, Y. Fu, and H. Chen, Nat. Rev. Mater. **1**, 16067 (2016).

[12] B. Yang, Q. Guo, B. Tremain, L. E. Barr, W. Gao, H. Liu, B. Béri, Y. Xiang, D. Fan, A. P. Hibbins, and S. Zhang, Nat. Commun. **8**, 97 (2017).

[13] L. H. Nicholls, F. J. Rodríguez-Fortuño, M. E. Nasir, R. M. Córdova-Castro, N. Olivier, G. A. Wurtz, and A. V. Zayats, Nat. Photon. **11**, 628 (2017).

[14] P. Wang, A. V. Krasavin, M. E. Nasir, W. Dickson, and A. V. Zayats, Nat. Nanotechnol. **13**, 159 (2018).

[15] C. Rizza, A. Di Falco, M. Scalora, and A. Ciattoni, Phys. Rev. Lett. **115**, 057401 (2015).

[16] Y. Li, S. Kita, P. Muñoz, O. Reshef, D. I. Vulis, M. Yin, M. Lončar, and E. Mazur, Nat. Photon. **9**, 738 (2015).

[17] M. H. Javani and M. I. Stockman, Phys. Rev. Lett. **117**, 107404 (2016).

[18] A. Ciattoni, C. Rizza, A. Marini, A. D. Falco, D. Faccio, and M. Scalora, Laser Photon. Rev. **10**, 517 (2016).

[19] I. Liberal, A. M. Mahmoud, Y. Li, B. Edwards, and N. Engheta, Science **355**, 1058 (2017).

[20] I. Liberal and N. Engheta, Nat. Photon. **11**, 149 (2017).

[21] S. Vezzoli, V. Bruno, C. DeVault, T. Roger, V. M. Shalaev, A. Boltasseva, M. Ferrera, M. Clerici, A. Dubietis, and D. Faccio, Phys. Rev. Lett. **120**, 043902 (2018).

[22] I. Liberal and N. Engheta, Proc. Natl. Acad. Sci. USA **115**, 2878 (2018).

[23] H. Chu, Q. Li, B. Liu, J. Luo, S. Sun, Z. H. Hang, L. Zhou, and Y. Lai, Light Sci. Appl. **7**, 50 (2018).

[24] A. R. Davoyan and N. Engheta, ACS Photon. **6**, 581 (2019).

[25] A. V. Goncharenko and K.-R. Chen, J. Nanophoton. **4**, 041530 (2010).

[26] A. V. Goncharenko and K.-R. Chen, J. Nanophoton. **4**, 040101 (2010).

[27] A. V. Goncharenko, V. U. Nazarov, and K.-R. Chen, Appl. Phys. Lett. **101**, 071907 (2012).

[28] A. V. Goncharenko, V. U. Nazarov, and K.-R. Chen, Opt. Mater. Express **3**, 143 (2013).

[29] A. V. Goncharenko, E. F. Venger, Y. C. Chang, and A. O. Pinchuk, Opt. Mater. Express **4**, 2310 (2014).

[30] L. Sun and K. W. Yu, J. Opt. Soc. Am. B **29**, 984 (2012).

[31] L. Sun and K. W. Yu, Appl. Phys. Lett. **100**, 261903 (2012).

[32] L. Sun, K. W. Yu, and X. Yang, Opt. Lett. **37**, 3096 (2012).

[33] L. Sun, J. Gao, and X. Yang, Phys. Rev. B **87**, 165134 (2013).

[34] L. Sun, X. Yang, and J. Gao, Appl. Phys. Lett. **103**, 201109 (2013).

[35] L. Sun, K. W. Yu, and G. P. Wang, Phys. Rev. Appl. **9**, 064020 (2018).

[36] Z. Hashin and S. Shtrikman, J. Mech. Phys. Solids **11**, 127 (1963).

[37] D. J. Bergman and Y. Imry, Phys. Rev. Lett. **39**, 1222 (1977).

[38] D. J. Bergman, Phys. Rep. **43**, 377 (1978).

[39] D. J. Bergman, Phys. Rev. Lett. **44**, 1285 (1980).

[40] G. W. Milton, Appl. Phys. Lett. **37**, 300 (1980).

[41] G. W. Milton, J. Appl. Phys. **52**, 5286 (1981).

[42] G. W. Milton, J. Appl. Phys. **52**, 5294 (1981).

[43] D. J. Bergman and D. Stroud, Solid State Phys. **46**, 147 (1992).

[44] G. W. Milton, *The Theory of Composites* (Cambridge University Press, Cambridge, England, 2002).

[45] S. Babar and J. H. Weaver, Appl. Opt. **54**, 477 (2015).

[46] T. C. Choy, *Effective Medium Theory: Principles and Applications* (Oxford University Press, Oxford, 2015).

[47] X. Chen, T. M. Grzegorczyk, B.-I. Wu, J. Pacheco, Jr., and J. A. Kong, Phys. Rev. E **70**, 016608 (2004).

[48] K. Kim and D. Stroud, Opt. Express **21**, 19834 (2013).